ELECTRIC-FIELD DISTRIBUTIONS OF DIELECTRIC SINGLE LAYERS OF SPHERES WITH DIFFERENT COMPACTNESS

A. Andueza[*], P. Morales, and J. Sevilla

Electric and Electronic Engineering Department, Universidad Pública de Navarra, Pamplona 31006, Spain

Abstract—The internal electric-field distribution from single layers of dielectric spheres with high refractive index ($n = 2.65$) has been analyzed for a number of different compactness cases by FDTD (Finite-Difference Time-Domain) method. The field distributions from the transmission spectra were compared with the internal electric-field distribution of the Mie modes of an isolated sphere. In general, the agreement is very good in almost all cases studied. The results show that TE and TM Mie modes are the origin of the resonances in the transmission spectra of the single layers. The resonances of the monolayer attributed to TE_{11} and TM_{11} Mie modes are only excited for compactness values lower than 0.38, suggesting a dependence of periodical arrangement effects for these modes. Moreover, the field distribution corresponding to some of the dips in the spectrum cannot be directly attributed to Mie modes (TE_{21}). The result indicates these are formed by degenerated or weakly coupled Mie modes induced by the periodic structure.

1. INTRODUCTION

Photonic Crystals generated a lot of expectation due to the intrinsic theoretical interest of periodic structures and, mostly, because the potential applications in the optical and microwave frequency ranges [1–4].

Among the different types of photonic crystals, periodic array of spheres is a fundamental one because of their electromagnetic behaviour and also because their construction possibilities and potential applications. The physical origin and the properties of the

photonic crystals based on dielectric spheres have been widely analyzed and investigated [5–29]. The transmission spectra for a single layer of dielectric spheres are characterized by a complex pattern of dips. These dips correspond to the photonic bands excited by incident electromagnetic waves. This photonic band effects are originated by the interplay of two elements: the morphology resonances by scattering Mie and the Bragg resonance caused by the periodic arrangement of the spheres [5]. Spheres are well-defined resonators that can be regarded as the photonic version of individual atoms in electronic crystals [5]. A photon in an isolated dielectric sphere is trapped like an electron in an atom due to the photon undergoes an attractive potential in the sphere. However, this confined photon can hop from one sphere to the neighbour by the optical tunnel effect. This coherent motion of the photon in the periodic lattice gives rise to the photonic band [7].

The transmission spectra of single layers of dielectric spheres present significant dips whose position and depth change with layer compactness [22, 24]. It is possible to discuss the origin of the photonic bands for an array of dielectric spheres by studying the electric-field intensity distribution. Since the photonic bands in the arrays of dielectrics spheres have their origin in Mie resonances of an isolated sphere, we can expect similarities between its field distribution and the one of the spheres immersed in a monolayer. This relation was pointed out in previous works [9], where its strong dependence with the spheres refractive index was studied. However, in [9] only two of the many dips of the spectra were studied. Our intention here is to extend this study to a larger number of picks in the spectra and to follow their variations with compactness.

Several single layers were selected, in triangular symmetry, varying the distance between the spheres to attain different compactness [24]. The transmission spectra and the electric-field distribution inside the spheres of these samples were numerically calculated by FTDT (Finite-difference time-domain) method. Calculated internal electric-field distributions for a single layer were compared with these for an isolated sphere, also obtained by FDTD calculations.

The most interesting conclusion of the numerical analysis is the extraordinary similarity of the electric field distribution for photonic bands and Mie modes for most of the resonances. As the layers become less compact, some new dips appear in the transmission spectra that were absent for higher compactness values. These resonances correspond to the lower order TE and TM Mie modes [30]. However, a significant discrepancy take place for one of the photonic bands studied, the same photonic band previously report as anomalous with compactness [25].

2. CALCULATION PROCEDURE

To obtain the internal electric-field distribution of the photonic bands for a single layer of dielectric spheres we considered a sample as shown Figure 1. The lattice geometry used was triangular, with a parameter notation: Φ for the sphere diameter and Λ to refer to the lattice constant, the separation between two consecutive centers in the unit cell. The dielectric constant of the spheres was selected to be $\varepsilon = 7$, similar to Soda Lime glass used in [22–26]. To indicate the compactness of a particular arrangement, filling factor parameter was used and denoted by ff. Filling factor is defined as the volume fraction that is occupied by spheres with respect to the total volume of a unit cell where the height equals the diameter of the sphere and it can be calculated as

$$ff = \frac{\pi}{3\sqrt{3}} \left(\frac{\Phi}{\Lambda}\right)^2 \tag{1}$$

We took the origin of coordinates as the center of one of the spheres, being x-y the plane where the spheres were arranged. All the calculations were performed for p polarization along x-axis of the single layer. The sampling plane is the one where the electric-field distribution was calculated and is shown by the broken line in Figure 1. It was selected parallel to x-y at a height of 0.2Φ from the origin of coordinates in x-y plane. The value of the sampling plane was similar to used by *Kurokawa et al.* [9], and was chosen in order to compare both results.

Due to the spherical symmetry of the sphere, Mie modes
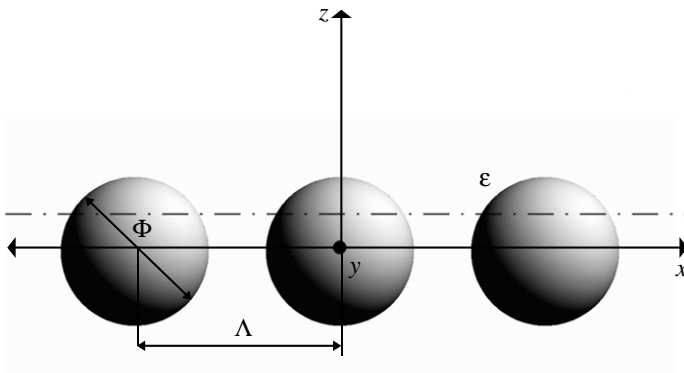
Figure 1. Geometrical arrangements used and parameters definition. The sampling plane is shown by the broken line.

(transverse electric or TE, and transverse magnetic or TM), are classified by angular momentum index (ℓ, m), where ℓ is the angular or mode number, m is the azimuth number. As m is equal to 1 in all cases, it is not taken into account. The same Mie mode (TE_ℓ or TM_ℓ) presents several frequencies of resonance [30, 31], so that we need other integer number to sort the resonances; this number is denoted by n. Therefore, we can define the Mie modes as $TE_{\ell,n}$ and $TM_{\ell,n}$, where ℓ is the mode number and n the order of the mode. For example, TE_{11} is the first order from the first TE Mie mode at $\Phi/\lambda = 0.353$ and TE_{12} is the second order from the first TE Mie mode $\Phi/\lambda = 0.739$.

In order to follow the strong dips observed in the transmission spectra for single layers of spheres of different compactness we introduce the "modes map" (Figure 2), a compact representation of the dips frequency position (in the vertical axis in dimensionless units) against compactness (presented as filling factor) [22, 24]. Horizontal dashed lines in Figure 2 represent the Mie modes, and the two dashed inclined curves are the first two orders of the Bragg frequency of the structure. Three influence regions can be defined into the modes
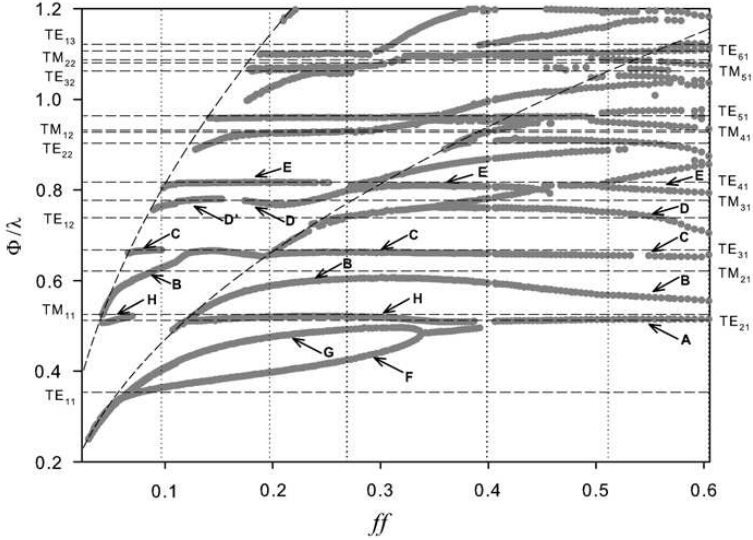
Figure 2. Modes map of 2D array of dielectric spheres in triangular arrangement at normal incidence. The analyzed modes pointed by arrows and represented by letters from A to H. Vertical and horizontal axes are the normalized frequency Φ/λ and ff respectively. Vertical dotted and horizontal dashed lines correspond to the samples calculated and Mie modes, respectively.

map [22, 24], high ($0.604 \geq ff > 0.4$), medium ($0.4 > ff > 0.12$) and low ($ff < 0.12$).

Several single layers with different values of compactness were considered for the analysis of the electric-field distribution. The values of Φ and Λ were selected for each ff value in a convenient way from modes map, fixing the similar diameter of spheres ($\Phi = 8\,\text{mm}$) and modifying the lattice period to obtain the ff value. The selected compactness samples were $ff = 0.6$, 0.51, 0.38, 0.27, 0.2 and 0.1, scanning every region of modes map as shown the Figure 2 [24]; high (0.604 and 0.51), medium (0.38, 0.27 and 0.197) and low (0.097).

Computer calculations were carried out using the CST Microwave Studio, a commercial code based on the FDTD method. This program is an electromagnetic field simulation software package specially suited for analysis and design in the high-frequency range. In our simulations absorption effects were neglected, remaining for the sphere material characterization only the dielectric permittivity, fixed always as $\varepsilon = 7$ ($n = 2.65$). All the calculation here presented corresponds to normal incidence. We only pay attention to normal incidence because it is enough to understand the performance of each band in the photonic crystal [9].

3. RESULTS AND DISCUSSION

In Figure 3 the transmission spectra calculated for samples of different compactness are presented. Sharp and broad dips can be seen in the frequency response of all the samples. The frequency is represented in every case normalized by sphere diameter (Φ/λ). The dips are labeled by letters A though H maintaining the same criteria as in Figure 2. Dips F, G and H, although correspond to the lowest frequencies, are only excited below certain compactness, for ff values lower than 0.38. We restrict our study to dips whose frequency (Φ/λ) is below 0.9, those well defined and clearly observable.

First, we discuss the internal electric-field distribution at the dip A for high values of compactness ($ff = 0.604$ and 0.51). The evolution of the dip A in the mode maps (see Figure 2) is quite flat and very close to TE_{21} Mie mode. This fact suggests that dip A is related with TE_{21} resonance of isolated sphere. Note that dip A disappears when the compactness value around 0.38 (see Figure 2), appearing at similar frequencies three new ones (F, G and H) at lower compactness values. The evolution of mode map suggests that dip A and dips F, G and H are related. This idea will be further analyzed.

The dip A is found in the spectra at $\Phi/\lambda = 0.514$ in Figure 4(a) and at $\Phi/\lambda = 0.513$ in Figure 4(b), around TE_{21} Mie
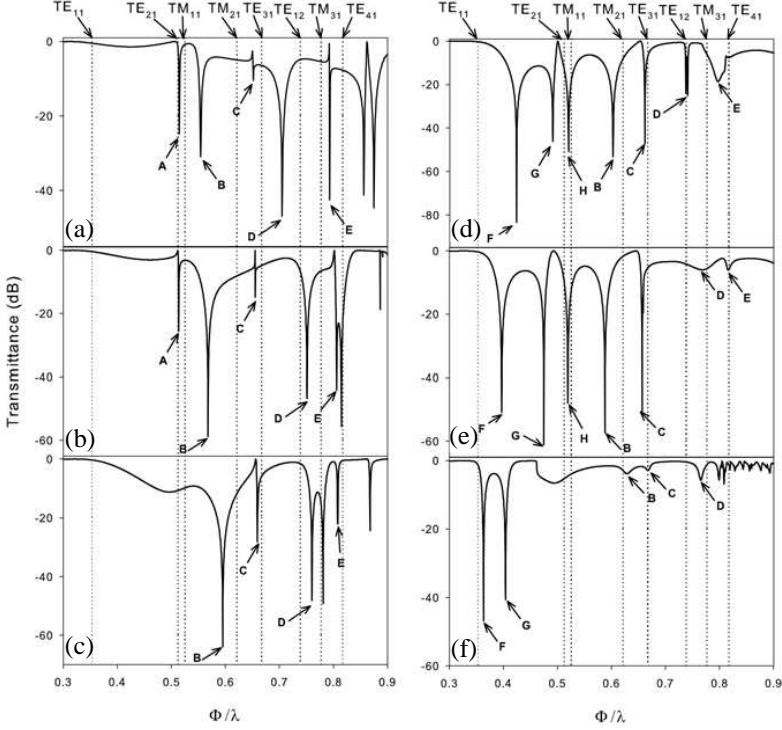
Figure 3. Transmission spectra of lattices with (a) $ff = 0.604$, (b) $ff = 0.51$, (c) $ff = 0.39$, (d) $ff = 0.27$, (e) $ff = 0.197$ and (f) $ff = 0.096$. Vertical dotted lines correspond to TE and TM frequencies of Mie resonances for an isolated sphere with dielectric permittivity $\varepsilon = 7$, and are shown in the top of the figures. Horizontal axis is the normalized frequency Φ/λ. The analyzed dips are represented by letters from A to H (same labels as in Figure 2).

resonance. Figures 4(a) to 4(b) show the internal electric-field intensity distribution at the dips A in the transmission spectra presented in Figures 3(a) and 3(b), respectively. Figures 4(c) and 4(d) correspond to the internal electric-field distribution of an isolated sphere TE_{21} and TM_{11} Mie modes. In all cases, darker region corresponds to the higher field intensity. Three regions of high intensity are located at the upper and lower edges and inside the sphere. The field distribution do not change significantly as the compactness decrease, their distribution remain constant for both lattices. Furthermore, the field is enhanced between spheres in the position where the spheres are in contact. The enhancement between the spheres is considered to be due to the strong interaction in close packed system [9].
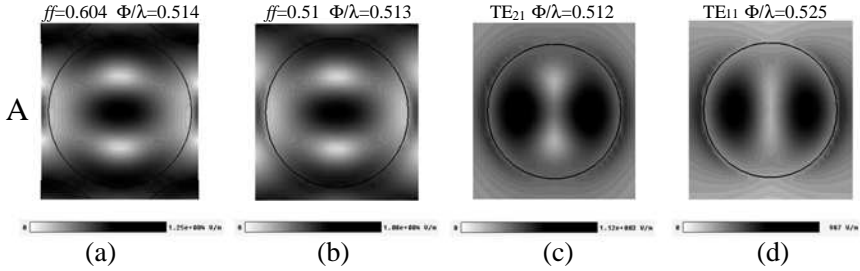
Figure 4. Distribution of the electric-field intensity distribution for dip A in a sphere. (a) $ff = 0.604$ at $\Phi/\lambda = 0.514$, (b) $ff = 0.51$ at $\Phi/\lambda = 0.513$, (c) an isolated sphere TE_{21} Mie mode at $\Phi/\lambda = 0.512$ and (d) an isolated sphere TM_{11} Mie mode at $\Phi/\lambda = 0.525$. The darker region corresponds to the higher field intensity.

Especially remarkable is the apparent mismatch in the field distribution between dip A and TE_{21} and TM_{11} Mie modes whose field distribution show two peaks inside the spheres (see Figures 4(c) and 4(d)). However, it can be noticed some similarity between the distributions in Figure 4. Indeed, there are two regions where the field is null between two maxima (see Figures 4(c) and 4(d)). However, these maxima seem to be merged in the monolayer (Figures 4(a) and 4(b)) while null field areas remain inalterable in all the cases in Figure 4. Furthermore, we can observe in Figures 3(a) and 3(b) how the dip A is near to TE_{21} mode in every compactness cases studied, but this proximity slightly varies from one ff value to other. These correspondences suggest that the characteristics of TE_{21} Mie resonances for an isolated sphere indeed appear in the dip A, although the data derived from electric-field distribution are not conclusive.

In Figure 5 there is presented the internal electric-field intensity distribution corresponding to dip C. The first picture (5(a) through 5(f)) correspond to single layers of progressively less compactness and the last one (Figure 5(g)) to the isolated sphere TE_{31} Mie mode. Note that the frequency evolution of dip C in the Mode map (see Figure 2) is quite flat and close to Mie resonance of the TE_{31}. Two crescent regions at the upper and low edges are shown in the electric filed distribution of all samples at dip C. Only the close packed sample (see Figure 5(a)), presents some mismatches, corresponding to two high intensity field distribution regions inside and between the spheres; that could be caused by the interaction between spheres in contact. Therefore we attribute the dip C to the Mie resonance of the TE_{31} mode. The internal field of this dip was previously studied by *Kurokawa et al.* [9]
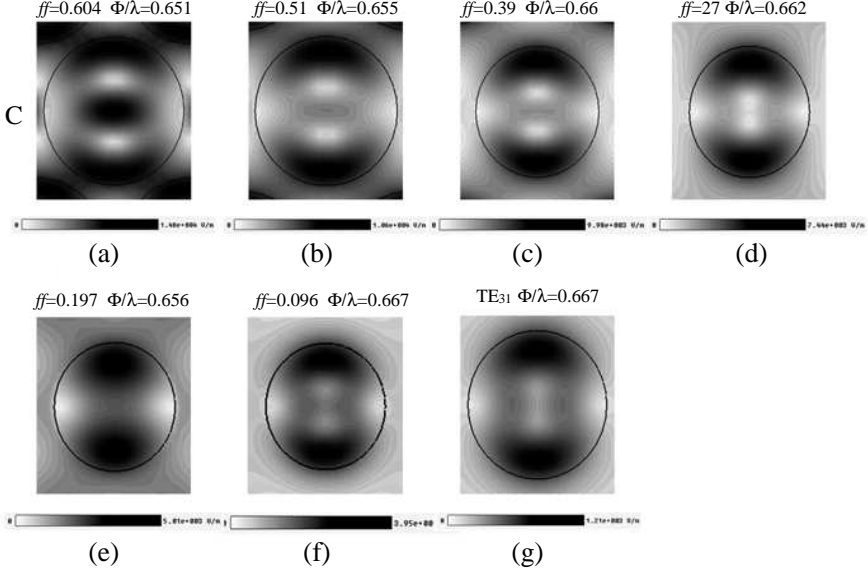
Figure 5. Distribution of the electric-field intensity for dip C in a sphere. (a) $ff = 0.604$ at $\Phi/\lambda = 0.651$, (b) $ff = 0.51$ at $\Phi/\lambda = 0.655$, (c) $ff = 0.39$ at $\Phi/\lambda = 0.66$, (d) $ff = 0.27$ at $\Phi/\lambda = 0.662$, (e) $ff = 0.197$ at $\Phi/\lambda = 0.656$, (f) $ff = 0.096$ at $\Phi/\lambda = 0.667$, and (g) an isolated sphere TE_{31} Mie mode at $\Phi/\lambda = 0.667$.

for spheres with a higher refractive index ($\varepsilon = 8.76$) and only for close packed samples, obtaining similar results.

For some other dips in the spectra, the analysis is very similar and lead to the same conclusion: a clear similarity between the internal field of the spheres in the singlelayer and the internal field distribution of Mie modes. Particularly, dips B, D and E can be correlated to Mie resonances TM_{21}, TM_{31} and TE_{41}, respectively. Although the figures corresponding to these dips have been calculated, are not included here to make the paper less cumbersome.

Let us focus now in the dips F, G and H, those that appear around the frequency of dip A below the compactness value of $ff = 0.4$ (See Figure 2 and Figure 3(c)). Figures from 6(a) to 6(c) show the internal electric-field intensity distribution at the dip F. The distributions present two darker regions at left-hand and right-hand sides of the sphere; as well as a significant region of high intensity outside of the sphere, that increases as the compactness of the lattices is lowered. The field distribution of an isolated sphere at the TE_{11} Mie mode is
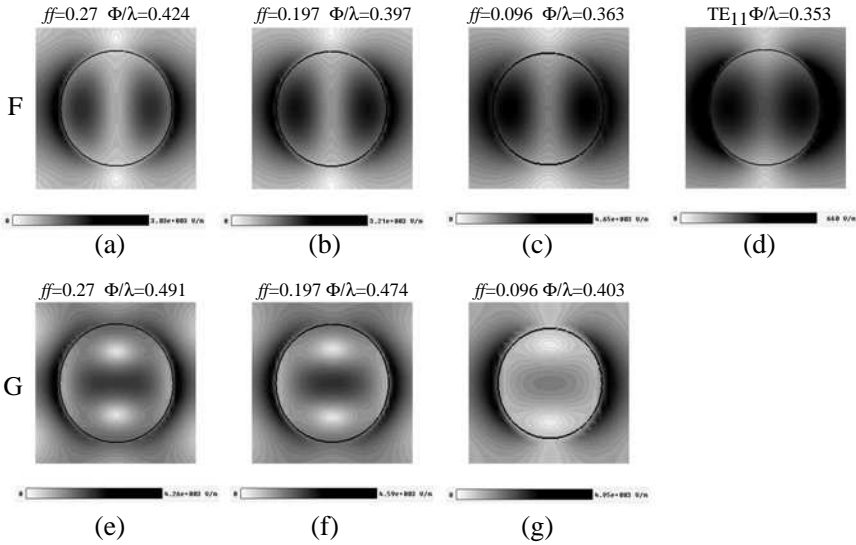
Figure 6. Distribution of the electric-field intensity for dips F and G in a sphere. (a) $ff = 0.27$ at $\Phi/\lambda = 0.424$, (b) $ff = 0.197$ at $\Phi/\lambda = 0.397$, (c) $ff = 0.096$ at $\Phi/\lambda = 0.363$, (d) an isolated sphere TE$_{11}$ Mie mode at $\Phi/\lambda = 0.353$, (e) $ff = 0.27$ at $\Phi/\lambda = 0.491$, (f) $ff = 0.197$ at $\Phi/\lambda = 0.474$ and (g) $ff = 0.096$ at $\Phi/\lambda = 0.403$.

shown in Figure 6(d). Although the influence of the Mie modes varies depending on compactness (the shape of the distribution for low values of compactness tends to be closer to TE$_{11}$ Mie Mode), in general the field distribution at the dip F is very similar to TE$_{11}$ Mie mode.

For dip G, Figures 6(e) to 6(g) present the distributions of electric-field intensity in samples of different compactness. We can observe that the internal electric-field distribution of the samples does not resemble any of the closer Mie modes: TM$_{11}$, TE$_{21}$ (Figures 4(c) and 4(d)) or TE$_{11}$ (Figure 6(d)). However, the electric field distribution of dip G is similar to the one of dip A. For instance, there are three regions of high intensity located at the upper and lower edges and inside the sphere. However, only a region of high intensity could be seen inside the sphere at the dip G. Note that two clear null field areas remain on both distributions. These correspondences suggest that the characteristics of the dip A indeed appear at the dip G, indicating that the two dips are closely related. This mode could be due to the existence collective states generated from the combination of single sphere ones [28]. In a previous work studying the evolution of the transmission spectra of these structures with positional disorder [25], dip G was identified

ff=0.27 Φ/λ=0.521   ff=0.197 Φ/λ=0.52   TE₁₁Φ/λ=0.525

H

3.54e+003 U/n   3.52e+003 U/n   987 U/n

(a)   (b)   (c)
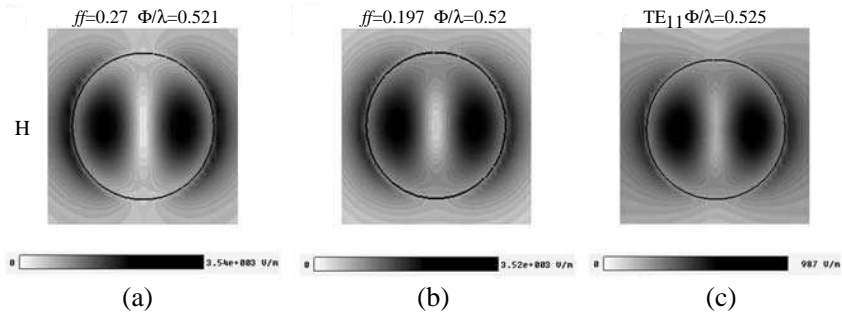
Figure 7. Distribution of the electric-field intensity for dip H in a sphere. (a) $ff = 0.27$ at $\Phi/\lambda = 0.521$, (b) $ff = 0.197$ at $\Phi/\lambda = 0.52$ and (c) an isolated sphere TM_{11} Mie mode at $\Phi/\lambda = 0.525$.

Table 1. Table of correspondence between transmission spectra dips and Mie modes.

Dip	Mie Mode
A	TE_{21}?
B	TM_{21}
C	TE_{31}
D	TM_{31}
E	TE_{41}
F	TE_{11}
G	TE_{21}?
H	TM_{11}

as significantly less tolerant to disorder, disappearing in lattices were other ones (F, B or C) remained clearly observable. From all this we conclude that dip G can not directly related to a single Mie mode TE_{21} and is highly dependent on the lattice structural arrangement.

Finally we present the simulation results for the dip H (Figure 7). The frequency position of this resonance is very close to the TM_{11} and TE_{21} Mie modes, as can be seen in Figure 2. The electrical field distribution corresponding to this resonance (dip H) in both studied compactness (Figures 7(a) and 7(b)) is almost identical to the one of TM_{11} Mie mode, shown in Figure 7(c). Therefore can be attributed the origin of dip H to TM_{11} Mie mode.

Summarizing, the correspondence between the electric field from

analyzed dips and Mie Modes is shown in Table 1. We have seen that the Mie resonances do play a significant role in the building up of the collective modes of spheres single layers, but not in a straightforward way. In general, most of the results obtained in the photonic bands are well described by tight-binding picture due to Mie resonances. In the case of the photonic bands from the monolayer, the model is based on superposition of Mie modes for an isolated sphere located at each lattice site. For a monolayer with high dielectric constant, the mixing between Mie modes of different order is relatively small and a typical picture of tight-binding bands applies well. It has been reported that this tight-binding picture based on spheres resonances holds well in the single layer of dielectric spheres with a large refractive index [16]. The analysis based on the internal electric-field distribution of the photonic bands from a monolayer, shows results coherent with the isolated sphere and tight-binding description. However, dips A and G present some discrepancies, since the field distributions are quite different from those of Mie modes of close frequencies. This could be due to the existence collective states generated from an isolated sphere states (TE_{21}) influenced by the periodic structure.

Finally, it is interesting to note that some of the photonic bands excited in a monolayer (dips F and H) appear when the compactness it is lower than 0.3. Regarding these results, we can establish that compactness turns out to be the reason of low frequency photonic bands, which are originated by lower Mie modes (TM_{11} and TE_{11}).

4. CONCLUSIONS

The internal electric-field distribution from triangular single layers of dielectric spheres with high refractive index ($n = 2.65$) has been calculated by FDTD method in a range of lattice compactness values. The same method was used to calculate the electric field distribution of the Mie modes of an isolated sphere. By comparing those distributions we have discussed the origin of the dips in the transmission spectra. The main conclusions that can be drawn from this study can be summarized in the following:

(i) Most of the photonic bands or dips are related with the TE and TM Mie modes, and their origin can be attributed to them through tight-binding picture.

(ii) The dips F and H of the monolayer can be attributed to TE_{11} and TM_{11} Mie modes, respectively. These dips are only excited for compactness values lower than 0.38, suggesting a total dependence of the low order Mie Modes with the distance between the spheres.

(iii) The field distribution from A and G dips cannot be clearly attributed to any Mie mode, in spite of TE_{21} mode could be related with them. The calculations indicate both dips are the same one, degenerated by the compactness effect. Therefore, these dips could be formed by hybrid or weakly coupled Mie modes, dominating by the periodic structure.

REFERENCES

1. Yablonovitch, E., "Inhibited spontaneous emission in solid-state physics and electronics," *Phys. Rev. Lett.*, Vol. 58, No. 20, 2059–2062, 1987.

2. John, S., "Strong localization of photons in certain disordered dielectric superlattices," *Phys. Rev. Lett.*, Vol. 58, No. 23, 2486–2489, 1987.

3. Joannopoulos, J. D., R. D. Meade, and J. N. Winn, *Photonic Cristal, Molding the Flow of Light*, Princeton University Press, New Yersey, 2005.

4. Soukoulis, C. M., *Photonic Band Gap Materialst*, Kluwer Academic Publishers, Dordrecht, 1996.

5. Miyazaki, H. and K. Ohtaka, "Near-field images of a monolayer of periodically arrayed dielectric spheres," *Phys. Rev. B*, Vol. 58, No. 11, 6920–6937, 1998.

6. Kondo, T., S. Yamaguti, M. Hangyo, K. Yamamoto, Y. Segawa, and K. Ohtaka, "Refractive index dependence of the transmission properties for a photonic crystal array of dielectric spheres," *Phys. Rev. B*, Vol. 70, No. 23, 1–6, 2004.

7. Kondo, T., M. Hangyo, S. Yamaguchi, S. Yano, Y. Segawa, and K. Ohtaka, "Transmission characteristics of a two-dimensional photonic crystal array of dielectric spheres using subterahertz time domain spectroscopy," *Phys. Rev. B*, Vol. 66, No. 3, 331111–331114, 2002.

8. Kurokawa, Y., Y. Jimba, and H. Miyazaki, "Optical band structure and near-field intensity of a periodically arrayed monolayer of dielectric spheres on dielectric substrate of finite thickness," *Phys. Rev. B*, Vol. 70, No. 15, 1551171–1551179, 2004.

9. Kurokawa, Y., Y. Jimba, and H. Miyazaki, "Internal electric-field intensity distribution of a monolayer of periodically arrayed dielectric spheres," *Phys. Rev. B*, Vol. 70, No. 15, 1550171–1550175, 2004.

10. Kurokawa, Y., H. Miyazaki, and Y. Jimba, "Light scattering from

a monolayer of periodically arrayed dielectric spheres on dielectric substrates," *Phys. Rev. B*, Vol. 65, No. 20, 2011021–2011024, 2002.

11. Kurokawa, Y., H. Miyazaki, H. T. Miyazaki, and Y. Jimba, "Effect of a semi-infinite substrate on the internal electric field intensity distribution of a monolayer of periodically arrayed dielectric spheres," *J. Phys. Soc. Jpn.*, Vol. 74, No. 3, 924–929, 2005.

12. Miyazaki, H. T., H. Miyazaki, K. Ohtaka, and T. Sato, "Photonic band in two-dimensional lattices of micrometer-sized spheres mechanically arranged under a scanning electron microscope," *J. Appl. Phys.*, Vol. 87, No. 10, 7152–7158, 2000.

13. Ohtaka, K., "Scattering theory of low-energy photon diffraction," *J. Phys. C*, Vol. 13, No. 4, 667–680, 1980.

14. Ohtaka, K., "Energy band of photons and low-energy photon diffraction," *Phys. Rev. B*, Vol. 19, No. 10, 5057–5067, 1979.

15. Ohtaka, K. and M. Inoue, "Light scattering from macroscopic spherical bodies. I. Integrated density of states of transverse electromagnetic fields," *Phys. Rev. B*, Vol. 25, No. 2, 677–688, 1982.

16. Ohtaka, K., S. Suda, T. Nagano, A. Ueta, T. Imada, T. Koda, J. S. Bae, K. Mizuno, S. Yano, and Y. Segawa, "Photonic band effects in a two-dimensional array of dielectric spheres in the millimeter-wave region," *Phys. Rev. B*, Vol. 61, No. 8, 5267–5279, 2000.

17. Ohtaka, K. and Y. Tanabe, "Photonic band using vector spherical waves. I. Various properties of bloch electric fields and heavy photons," *J. Phys. Soc. Jpn.*, Vol. 65, No. 7, 2265–2275, 1996.

18. Ohtaka, K. and Y. Tanabe, "Photonic bands using vector spherical waves. II. Reflectivity, coherence and local field," *J. Phys. Soc. Jpn.*, Vol. 65, No. 7, 2276–2284, 1996.

19. Ohtaka, K. and Y. Tanabe, "Photonic bands using vector spherical waves. III. Group-theoretical treatment," *J. Phys. Soc. Jpn.*, Vol. 65, No. 8, 2670–2684, 1996.

20. Sainidou, R., N. Stefanou, I. E. Psarobas, and A. Modinos, "Scattering of elastic waves by a periodic monolayer of spheres," *Phys. Rev. B*, Vol. 66, No. 2,, 243031–243037, 2002.

21. Yano, S., Y. Segawa, J. S. Bae, K. Mizuno, S. Yamaguchi, and K. Ohtaka, "Optical properties of monolayer lattice and three-dimensional photonic crystals using dielectric spheres," *Phys. Rev. B*, Vol. 66, No. 7, 751191–751197, 2002.

22. Andueza, A., R. Echeverria, and J. Sevilla, "Evolution of the electromagnetic modes of a single layer of dielectric spheres with

compactness," *J. Appl. Phys.*, Vol. 104, No. 4, 043103, 2008.

23. Andueza, A. and J. Sevilla, "Non compact single-layers of dielectric spheres electromagnetic behaviour," *Opt. Quantum Electron.*, Vol. 39, Nos. 4–6, 311–320, 2007.

24. Andueza, A., R. Echeverria, P. Morales, and J. Sevilla, "Geometry influence on the transmission spectra of dielectric single layers of spheres with different compactness," *J. Appl. Phys.*, Vol. 107, No. 12, 124902, 2010.

25. Andueza, A., T. Smet, P. Morales, and J. Sevilla, "Disorder effect in the transmission spectra of a noncompact single layer of dielectric spheres derived from microwave spectroscopy," *Appl. Opt.*, Vol. 50, No. 31, 91–97, 2011.

26. Andueza, A., P. Morales, and J. Sevilla, "Photonic band effect in single-layers of high refractive index spheres of different compactness," *J. Appl. Phys.*, Vol. 111, No. 10, 104902, 2012.

27. Handapangoda, C. C., M. Premaratne, and P. N. Pathirana, "Plane wave scattering by a spherical dielectric particle in motion: A relativistic extension of the Mie theory," *Progress In Electromagnetics Research*, Vol. 112, 349–379, 2011.

28. Lidorikis, E., M. M. Sigalas, E. N. Economou, and C. M. Soukoulis, "Tight-binding parametrization for photonic band gap materials," *Phys. Rev. Lett.*, Vol. 81, No. 7, 1405–1408, 1998.

29. Shalin, A. S., "Optical antireflection of a medium by nanostructural layers," *Progress In Electromagnetics Research B*, Vol. 31, 45–66, 2011.

30. Mie, G., "Die optischen eigenschaften kolloider goldlsungen," *Zeitschrift für Chemie und Industrie der Kolloide*, Vol. 2, No. 5, 129–133, 1907.

31. Bohrem, C. F. and D. R. Huffman, *Absorption and Scattering of Light by Small Particules*, Wiley, New York, 1995.